JOURNAL OF GEOPHYSICAL RESEARCH, VOL. 105, NO. C5, PAGES 11,243–11,258, MAY 15, 2000

A diagnostic study of the Indonesian Throughflow

Konstantin V. Lebedev[1] and Maxim I. Yaremchuk[1]
International Pacific Research Center, University of Hawaii, Honolulu

Abstract. The objective of this study is to derive estimates of the mean seasonal variations in the Pacific to Indian Ocean throughflow transport using climatological data of the temperature/salinity fields and surface wind stress. A variable grid global general circulation model (GCM) with 1/6° resolution in Indonesian seas configured with ETOP05 bottom topography is utilized to diagnose the three-dimensional velocity field. An extensive set of sensitivity experiments is conducted to obtain estimates of the error bars. The computations show that Indonesian Throughflow (ITF) is maximum in boreal summer (13.9±1.3 Sv) and minimum in boreal winter (7.5±1.1 Sv). The annual mean ITF transport amounts to 11.5±1.1 Sv (1 Sv=10^6 m^3 s^{-1}). These values are within the range of various estimations of ITF transport, and they agree in phase. The largest seasonal variations of the transport occur in the upper 175 m of the water column, exhibiting a 8 Sv amplitude of the seasonal cycle. This causes a substantial variability in the heat transport from the Pacific to the Indian Ocean. Its value increases from 0.4±0.1 PW in January to 1.1±0.1 PW in August (1 PW=10^{15} watts). In contrast to previous GCM-based studies, the annual mean transport is found to be more evenly distributed among the three major outlets from the Indonesian seas (Lombok, Ombai, and Timor Straits). The Luzon Strait inflow gives a considerable contribution to ITF. In winter the inflow of 6.3±1.5 is distributed between the two outflows from South China Sea, which follow the routes through Karimata (4.4±0.5) and Mindoro (1.9±1.5 Sv) Straits. In summer the Karimata pathway is blocked, and the net inflow of 4.7±0.6 Sv exits through the Mindoro Strait west of southern Luzon. The total contribution of the Luzon Strait inflow to the net ITF transport varies from 85% in boreal winter to 35% in summer, with an annual average value of ~50%. Cross-correlation analysis of the TOPEX/Poseidon monthly mean sea surface height (SSH) anomalies and the diagnosed transport anomalies demonstrates high correlation of the mean SSH difference between the regions in western Banda Sea and north of Luzon with the heat (0.96) and volume (0.91) transports.

1. Introduction

In recent years, Indonesian Throughflow (ITF) variability has been discussed in a large number of papers. This interest is primarily due to the important role ITF plays in the thermohaline balance of the Pacific and Indian Oceans and possibly in the global climate system. However, the net ITF volume transport and its variability still have not been adequately quantified because of the lack of observations in the Indonesian territorial waters. A comprehensive overview of the ITF transport estimates based on direct measurements has been given recently by *Gordon and McClean* [1999], who conclude that the [*Gordon and McClean*, 1999, p. 202] "prevailing wisdom seems to point to 5-10 Sv annual average throughflow with the maximum transport occurring during the southeast monsoon (August)." This conclusion has been derived from the results cited in more than 20 papers covering the period 1981–1996. The "RMS variance" of these estimates is, however, close to 10 Sv so that the problem of the ITF quantitative assessment still cannot be considered as solved.

Because of sparsity of data, a large number of recent ITF studies have been focused on the analysis of the output produced by general circulation model (GCM) simulations for the region with increasing resolutions. *Miyama et al.* [1995] obtained the annual mean ITF transport of 20±3 Sv using the 19-level 1/2°×1/2° ocean general circulation model (OGCM) with Digital Bathymetric Data Base 5 (DBDB5) topography. *Murtugudde et al.* [1998] utilized a 9-level 2/3°×1/3° model

[1]Also at Shirshov Institute of Oceanology, Moscow, Russia.

Paper number 2000JC900015.
0148-0227/00/2000JC900015$09.00

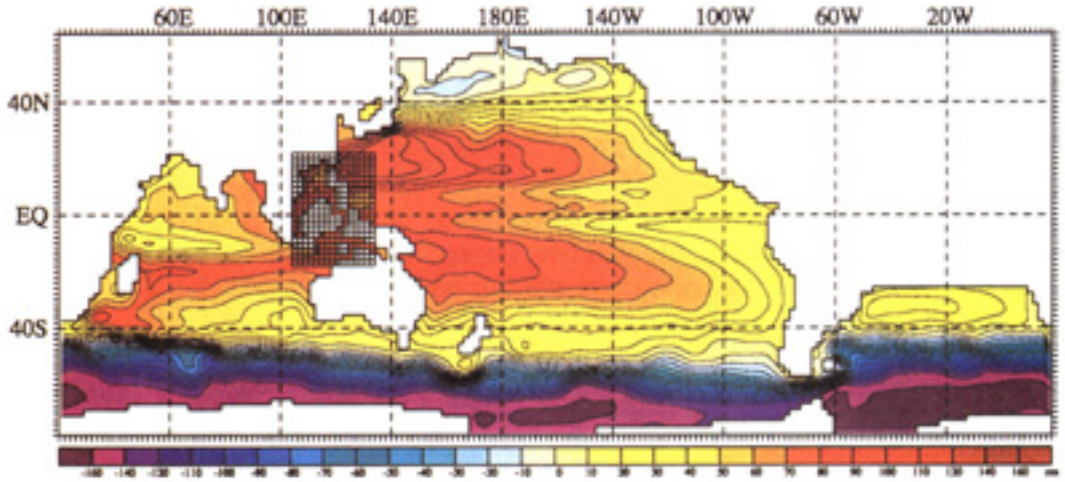

Plate 1. The global annual mean sea surface height diagnostically derived from the climatological data. The hatched rectangle denotes the region Ω with $1/6^\circ \times 1/6^\circ$ resolution.

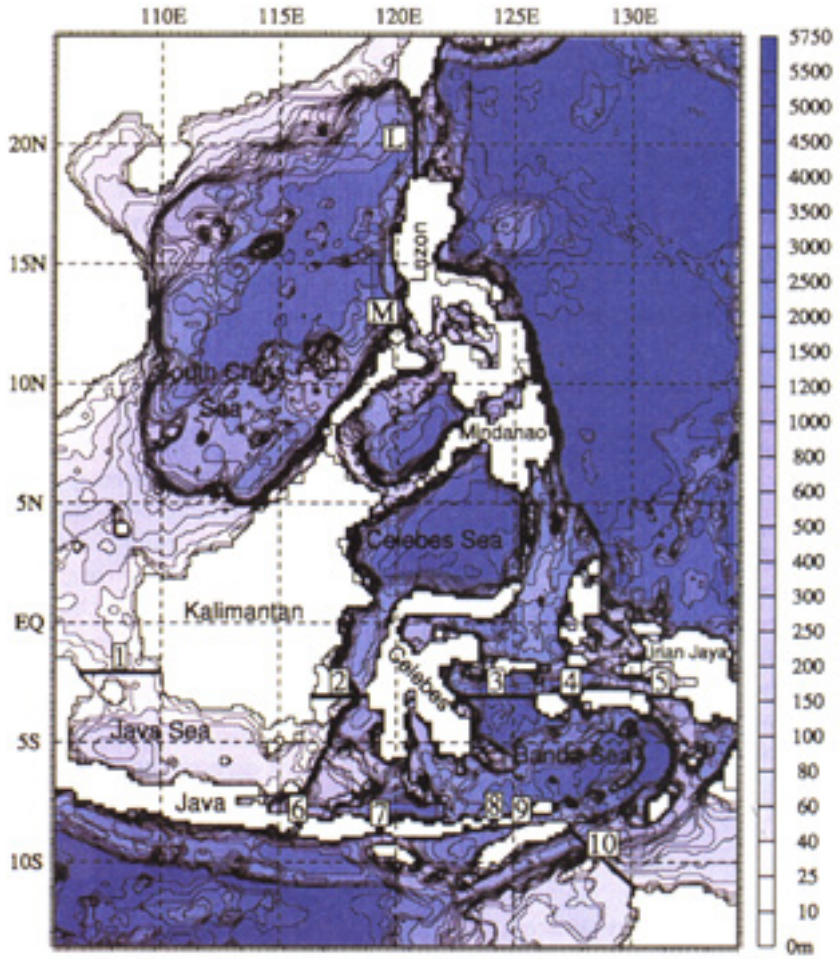

Plate 2. Model topography (meters). Solid lines indicate the key "inflow" (1-5) and "outflow" (6-10) straits. The numbers correspond to those in Table 1. Additionally, the Luzon Strait (L) (cross-section area of 630 km^2), and the Mindoro Strait (M) (cross-section area of 26 km^2) are shown.

to study seasonal effects of the ITF on the tropical Indo-Pacific basin. In their simulations the net ITF transport varied between 8 Sv in June-July and 0 Sv in December-January. *Schiller et al.* [1998] obtained 16.3 Sv flowing on the average into the Indian Ocean in their global OGCM. The net ITF heat transport was directed from the western Pacific and had a value of 1.15 PW. The coupled ocean-atmosphere GCM used by *Schneider and Barnett* [1997] produced 13.1 Sv and 0.9 PW. *Potemra et al.* [1997] analyzed the output of a 20-level 0.4° OGCM of *Semtner and Chervin* [1992]. Between 1987 and 1996 the simulated transport varied in the range of 11–4 Sv with maxima in August and minima in January. Later, *Potemra* [2000] studied seasonal variability of the ITF using a relatively simple $1\frac{1}{2}$ -layer model, forced by Hellerman wind stress with resolutions from 1° to 1/6°, and obtained the annual mean transport of 10±1 Sv.

Recently, *Gordon and McClean* [1999] examined the output of a 20-level 1/4° simulation produced by the Parallel Ocean Program (POP) global ocean model. The model transport varied between 7 Sv in August 1993 and 0.6 Sv in February 1994 with a net average heat transport of 0.66 PW. Gordon and McClean pointed out a number of substantial discrepancies between the simulated hydrographic fields and the ones directly observed within the framework of the Arlindo Project in 1993. For instance, model temperature was 3°C warmer in the 200–1200 dbar interval, while in the 5°–28°C temperature range, salinity was excessive, often by more than 0.2 practical salinity units (Psu). Besides, Gordon and McClean pointed out a number of unrealistic features in bottom topography, which might have had a substantial influence on the integral ITF properties.

Having in mind the above mentioned model/data inconsistencies, which may be typical of the results of long-term integrations of high resolution GCMs, we are making an attempt to utilize an alternative approach of "robust diagnostic modeling," which relies more heavily on data. The last work of this type was done by *Miyama et al.* [1995], who used a much coarser grid employing a GCM of the Bryan-Cox type.

In the present study we combine dynamical interpolation properties of a high-resolution OGCM with the *Levitus and Boyer* [1994] and *Hellerman and Rosenstein* [1983] monthly mean climatologies to study the spatial structure of the ITF and its seasonal variability. In contrast to previous modeling studies known in literature, we utilize a finer horizontal resolution of 1/6° in Indonesian seas with 32 layers in the vertical. Additionally, a more realistic bottom topography derived from the ETOP05 database is used. Such a "refined" formulation enabled us to obtain much more realistic topography in the key straits across the Lesser Sunda Islands governing ITF at 8.5°S. We also conduct an extensive set of sensitivity experiments to examine the effect of wind forcing and subgrid scale parameterization on the diagnostic patterns. Correlations of the diagnosed ITF transports with the TOPEX/Poseidon altimetry are also established.

The paper is organized as follows. In the next section the numerical model and the diagnostic method are described. Special emphasis is given to the description of bottom topography in the region of Indonesian seas and to the results of sensitivity experiments aimed at evaluation of the error bars. In section 3 the features of seasonal cycle in the velocity fields are given. In section 4, correlation of the transports with altimetric data are described, and in section 5 results are discussed and summarized.

2. Description of the Method

2.1. Data

The model region in this study covers the entire globe excluding the Arctic and Atlantic Ocean north of 25°S (Plate 1). Vertically, the model domain is divided into 32 levels of variable separation from 10 m in the upper ocean to 500 m in the deep ocean. The levels coincide with those of *Levitus and Boyer* [1994] climatology. In the horizontal we use the grid with variable steps. The finest resolution of 1/6° both in latitude and longitude is prescribed for the region Ω bounded by 15°S–25°N and 105°–135°E, respectively (Plate 1). Outside that area, grid spacing gradually increases to 2° in the "transition zones" 15° wide.

The study is based on ETOP05 topographic data National Oceanic and Atmospheric Administration (NOAA) [1986], which has the global resolution of 1/12° (`http://web.ngdc.noaa.gov/mgg/global/seltopo.html`). The model topography (Plate 2) was obtained by averaging ETOP05 values over the model grid cells. Because topography seems to play a decisive role in governing the ITF, we tried to preserve the most accurate possible representation of the bottom relief in the Indonesian seas, with special focus on the straits between Lesser Sunda Islands and east of Timor. In particular, ETOP05 data show an extremely shallow sill in the Torres Strait with a number of "channels" 2-10 m deep winding among the coral reefs. The total effective cross-section area of the strait does not exceed 0.2 km^2. Taking into the account additional considerations by *Gordon and McClean* [1999], we decided to close Torres Strait in our model configuration. Table 1 gives a comparison of the section areas of the key straits characterizing the 0.4° Parallel Ocean Climate Model (POCM) configuration used by *Potemra et al.* [1997], our model topography, and the ETOP05 data set.

Monthly winds of *Hellerman and Rosenstein* [1983] (hereinafter referred to as HR) and hydrographic climatology of *Levitus and Boyer* [1994] are available with coarser resolution. They were interpolated onto finer grids using bicubic splines. The same type of interpolation was used in sensitivity experiments for projecting other wind stress climatologies onto the model grid.

Table 1. Cross-Section Areas of the Key Straits

	Strait	ETOP05	POCM	Model
1	Karimata	10.8	22	11
2	Makassar	90.7	56	93
3	Molucca	1509.5	1432	1450
4	Manipa	52.1	98	50
5	Ceram	194.6	195	208
6	Lombok	32.6	30	33
7	Komodo	4.8	—	5
8	Lomblen	4.9	—	5
9	Ombai	62.2	196	58
10	Timor	256.2	233	260
11	Torres	0.2	15	—
12	Sunda	0.1	7	—

Areas are in km^2. POCM, Parallel Ocean Climate Model.

Figure 1 shows the mean wind stress over Ω derived by averaging over the ensemble of six different climatological wind fields listed in Table 2 (section 2.3). It is of note that the RMS variance of the wind stress climatologies over the ensemble is 0.26 dyn cm^{-2} (or 35% of the typical wind stress magnitude within Ω).

2.2. Model

In our computations we have used an OGCM designed on the basis of the Bryan-Cox model by *Demin and Ibraev* [1989]. Technically, the code is analogous to the surface pressure formulation suggested by *Smith et al.* [1992] and *Dukowicz et al.* [1993]. The major advantage of the sea surface height (SSH) formulation is the absence of difficulties connected with the treatment of multiply connected domains in the original stream function formulation of the model. Under the rigid lid, Boussinesq and hydrostatic approximations the governing equations are

$$\mathbf{u}_t + (\mathbf{u}\cdot\nabla)\mathbf{u} + w\mathbf{u}_z + f(\boldsymbol{k}\times\mathbf{u}) + \frac{1}{\rho_0}\nabla p - $$
$$-(\nabla\cdot D_m\nabla)\mathbf{u} - (K_m\mathbf{u}_z)_z = \mathbf{F}_u, \quad (1)$$
$$p_z + g\rho = 0, \quad (2)$$
$$\nabla\mathbf{u} + w_z = 0, \quad (3)$$
$$\theta_t + \nabla(\mathbf{u}\theta) + (w\theta)_z -$$
$$-(K_\theta\theta_z)_z - (\nabla\cdot D_\theta\nabla)\theta - \hat{\Pi}_\rho\theta = F_\theta, \quad (4)$$
$$S_t + \nabla(\mathbf{u}S) + (wS)_z -$$
$$-(K_S S_z)_z - (\nabla\cdot D_S\nabla)S - \hat{\Pi}_\rho S = F_S, \quad (5)$$
$$\rho - \mathcal{R}(\theta, S, p) = 0, \quad (6)$$

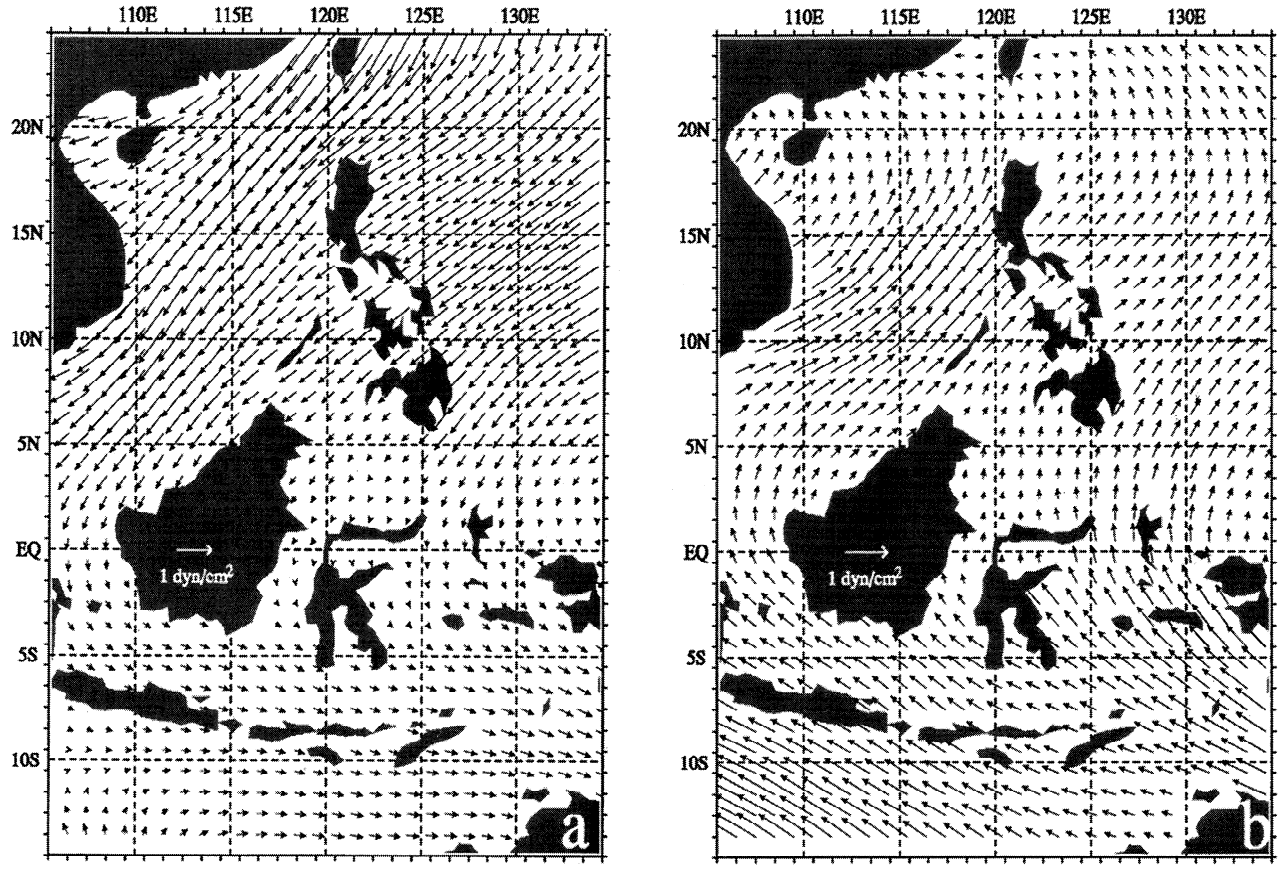

Figure 1. Mean climatological wind stress field in boreal (a) winter and (b) summer. The averaging was done over six wind stress climatologies for January–March and July–September periods.

Table 2. Total Indonesian Throughflow (ITF) Transports of Mass, Heat, and Salt Diagnosed Using Different Wind Climatologies

Winds	Mass, Sv	Heat, PW	Salt, Tg s^{-1}
HR	12.7	0.90	0.45
RHR	11.0	0.80	0.39
NOGAPS	10.9	0.78	0.38
ECMWF	12.3	0.89	0.43
COADS	11.7	0.85	0.41
NCEP	10.4	0.78	0.36
mean$\pm\sigma_\tau$	11.5±0.8	0.83±0.05	0.40±0.03

HR, *Hellerman and Rosenstein* [1983]; RHR, reduced Hellerman; NOGAPS, Navy Operational Global Atmospheric Prediction System; ECMWF, European Centre for Medium-Range Weather Forecasts; COADS, Comprehensive Ocean-Atmosphere Data Set; and NCEP, National Centers for Evironmental Prediction.

where $\mathbf{u} \equiv (u, v)$ and w are the horizontal and vertical velocity components, respectively, θ is potential temperature, S is salinity, p is pressure, ρ_0 and ρ are the mean density and deviation from that mean, g is the gravitational acceleration, f is the Coriolis parameter, K_m and D_m and $K_{\theta,S}$ and $D_{\theta,S}$ denote the vertical and horizontal diffusion coefficients for momentum, θ, and S, ∇ stands for the horizontal gradient operator, and $\hat{\Pi}_\rho$, $\mathcal{R}$, $\mathbf{F}_u$, F_θ, and F_S represent symbolically the convective adjustment operator, the equation of sea water state, and surface forcings.

To improve the model performance and following the ideology of "implicit free surface" approach given by *Dukowicz and Smith* [1994], we have modified the diagnostic equation for the free surface elevation ζ by changing the rigid lid condition for vertical velocity to a free surface formulation. The Coriolis term in the ζ equation was treated semi-implicitly.

The other model parameters were set as follows. Horizontal diffusion of temperature, salinity, and momentum was unisotropic and D_m and $D_{\theta,S}$ varied horizontally according to the relationships

$$D^i_m = d_m \Delta x^i / 2^\circ \qquad D^i_{\theta,S} = d_{\theta,S} \Delta x^i / 2^\circ,$$

where Δx^i is the local grid spacing along the ith direction in degrees, d_m=400 m^2 s^{-1}, and $d_{\theta,S}$=200 m^2 s^{-1}. Therefore diffusion coefficients used within Ω were D_m= 33 and $D_{\theta,S}$=17 m^2 s^{-1}. The following values for the vertical momentum and tracer diffusion were used: K_m=10^{-3} m^2 s^{-1} and $K_{\theta,S}$=10^{-4} m^2 s^{-1}. The magnitudes of d_m, $d_{\theta,S}$, K_m, and $K_{\theta,S}$ were varied in the course of sensitivity experiments. The equation of state for seawater was taken in the form of *Ishizaki*'s [1994] approximation to the United Nations Educational Scientific, and Cultoral Organization (UNESCO) [1981] formula.

The boundary conditions were as follows. At the sea surface we specify the Dirichlet boundary condition for potential temperature and salinity, taking them from Levitus climatology [*Levitus and Boyer*, 1994]. Surface momentum flux is imposed on the basis of wind stress climatology. At the rigid boundaries of the domain, zero normal fluxes of mass, temperature, salinity, and the tangent momentum component were prescribed. Open boundaries at the Bering Strait and along 25°S in the Atlantic were treated as rigid.

2.3. Diagnostic Technique and Sensitivity Experiments

A straightforward way to investigate circulation in the ITF region is to integrate the model equations for 20-30 years until the model reaches a kind of statistical equilibrium. This approach has been taken by many, but it may sometimes lead to unrealistically large deviations of the thermohaline structure from the climatologies. These discrepancies may be caused by errors in the forcing fields and/or by small model deficiencies that may amplify significantly during long integration. On the other hand, the model can be nudged to climatology using a robust diagnostic method of *Sarmiento and Bryan* [1982] (an approach taken by *Miyama et al.* [1995]). In that case, model physics may be distorted significantly because of the presence of artificial three-dimensional (3-D) sources of heat and salt in the tracer transport equations.

The third approach can be considered as an intermediate one. It is usually referred to as the semidiagnostic technique and is often used in meteorology [e.g., *Washington and Parkinson*, 1986, *Pitcher et al.*, 1983] and oceanography [e.g., *Ivanov et al.*, 1997]. Data analysis is performed in two steps. At the first step the model velocity field is adjusted to θ/S climatologies via forcing the equations (1)–(3) by the corresponding steady state climatological winds and integrating them forward in time until all the fast transient processes are damped. After that the model (1)–(6) is allowed to evolve freely under the stationary climatological forcing fields at the surface. The integration is terminated after ~300-350 days. This time is sufficient to remove fast trends from the solution, so that RMS values of temporal derivatives become consistent with the climatological timescale. On the other hand the solution does not deviate too far from data. In our computations the integration time was defined to satisfy three criteria simultaneously: (1) the RMS value of the temporal variability timescale in Ω is >150 days; (2) the RMS variability, computed over the last 60 days of integration, of the heat, salt and volume transports through 10 sections shown in Plate 2 does not exceed 0.2 Sv, 0.02 PW, and 0.01 Tg s^{-1}; and (3) the RMS deviations of the potential temperature and salinity fields from their monthly mean climatological values do not exceed 20% of the RMS spatial variability of the climatologies.

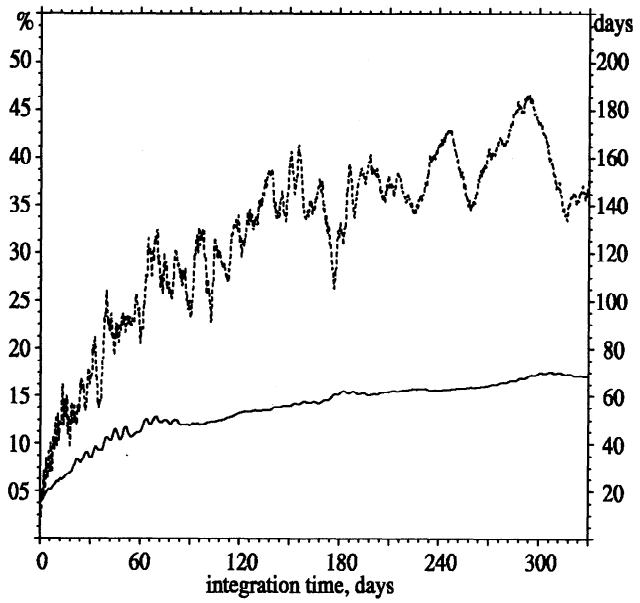

Figure 2. Evolution of ϵ (solid line) and T in the diagnostic run for reduced Hellerman (RHR) November mean climatology.

Figure 2 demonstrates typical evolution with time of the mean relative error of the potential temperature and salinity fields within the domain Ω with 1/6° resolution. The relative error ϵ was computed by the formula

$$\epsilon = \frac{1}{2}\langle \frac{\sigma'(\theta-\theta_c)}{\sigma(\theta_c)} + \frac{\sigma'(S-S_c)}{\sigma(S_c)} \rangle \qquad (7)$$

$$\sigma'(\varphi) \equiv [\overline{\varphi^2}]^{\frac{1}{2}} \qquad \sigma(\varphi) \equiv [\overline{(\varphi-\overline{\varphi})^2}]^{\frac{1}{2}}$$

Here subscript c denotes climatology, while angular brackets and overbars stand for the depth average and horizontal mean over Ω, respectively. As it is seen from Figure 2, rapid error growth decreases considerably after the first 50 days of integration. A linear trend of $\sim$6% yr^{-1}, however, remains persistent up to the end of a 1 year integration period.

Temporal variability timescale T computed as

$$T = \frac{1}{2}\langle \frac{\sigma(\theta_c)}{\sigma'(\partial_t\theta)} + \frac{\sigma(S_c)}{\sigma'(\partial_t S)} \rangle$$

does not rise higher than 190 days, generally as a result of persistent eddy formation southeast of Mindanao and in the deep areas of the South China Sea. Nevertheless, these nonlinear processes do not seem to affect significantly the values of total ITF transports (Figure 3) whose temporal variability reduces by an order in magnitude after approximately half a year of integration. Figures 2-3 are typical of all the diagnostic runs. In most of the cases, integration was terminated after 300-350, days when all the three outlined above conditions were met.

To suppress local features associated with eddy activity, the final diagnostic patterns have been derived as temporal averages of the ocean state over the last 60 days of integration. The computations have been performed for 12 monthly mean HR and "reduced Hellerman" (RHR) climatologies. The RHR set was obtained by multiplying HR winds by the factor of 0.75 (as recommended by the Tropical Ocean-Global Atmosphere/Numerical Experimental Group [*Stockdale et al.*, 1993, *Masumoto and Yamagata*, 1993, 1996]). Five additional runs were made to check the reliability of the results. These were done using seasonal and annual mean HR and RHR climatological data. As will be discussed in section 3, property transports through the key straits, computed from these runs are consistent with those obtained via processing of the monthly climatologies. Actual circulation patterns are also highly consistent with each other when averaged over a corresponding season (year) and appear to be almost identical from the qualitative point of view.

Figure 4 shows the results of three 20 year experiments using the diagnostic method of *Sarmiento and Bryan* [1982] with varying magnitude of the nudging term factor γ. The experiments were made using HR winds. The first experiment was done in the "free evolution mode" with γ=0 (no artificial model/data misfit terms in θ/S equations). In two other experiments the values of γ were taken as 1/100 and 1/400 days. As is seen, in the "free evolution" experiment, ITF transport reaches its asymptotic value of 9.5 Sv after 13 years of integration. At the same time on the 13th year of integration, model θ/S fields deviate too far (by 40%) from their climatological values. The major error contribution comes from salinities below 200 m and temperatures at the intermediate levels. In the "strong" and "weak" nudging modes, model/data discrepancies are

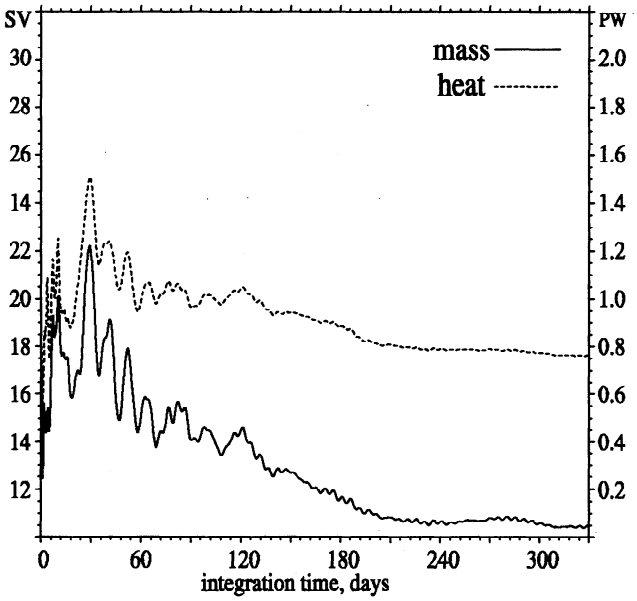

Figure 3. Evolution of the net mass (solid line) and heat Indonesian Throughflow (ITF) transports in the diagnostic run for RHR November mean climatology.

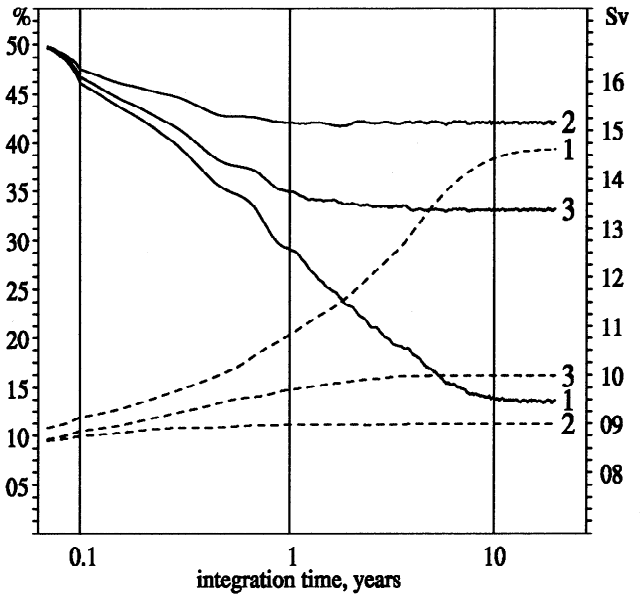

Figure 4. Evolution of the low-pass filtered net ITF transports (solid lines) and the mean θ/S deviations from climatology (dashed lines) in the "free run" (1) and in runs with $\gamma = 1/100$ days (2) and $\gamma = 1/400$ days (3).

under control, so that errors do not exceed acceptable values of 10–20%. Nevertheless, simple estimates show that the nudging terms dominate over physical terms in the left-hand sides of the tracer evolution equations and may have a significant influence on the flow physics, especially at long timescales. As was mentioned earlier, in the present study we follow an "intermediate approach," keeping a reasonable balance between the faith in model skill and in hydrological data. We believe that Levitus climatology contains considerable information on the long-term oceanic response to surface forcing. Consequently, we chose to terminate model integration after a relatively short period of time in favor of keeping the solution close to hydrological data.

To study sensitivity of the results to variations of the wind forcing and diffusion parameters, we have conducted four series of additional runs with various wind stress climatologies and a set of six runs with varying diffusion coefficients. The major purpose of these computations was to establish approximate error bars for the ITF transports. Each of the four series of wind sensitivity experiments consisted of five diagnostic runs forced by the seasonal and annual mean winds. The four series were made with European Centre for Medium-Range Weather Forecasts (ECMWF) [*Trenberth et al.*, 1989, 1990], Navy Operational Global Atmospheric Prediction System (NOGAPS) [*Goerss and Phoebus*, 1992], Comprehensive Ocean-Atmosphere Data Set (COADS) [*Da Silva*, 1995], and National Centers for Evironmental Prediction (NCEP)/National Center for Atmospheric Research (NCAR) wind stress climatologies. Sensitivity of the net ITF transports to wind forcing is shown in Table 2.

The diffusion sensitivity series was done with HR seasonal and annual winds for six combinations of the diffusion coefficients shown in Table 3. As is seen, the algorithm is weakly sensitive to variations of the diffusion coefficients within an order of magnitude. The transports vary within 3–7% of their mean values, resembling the results of *Inoue and Welsh* [1993] and *Potemra* [2000]. Nevertheless, transport uncertainties attributed to diffusion are comparable in magnitude with the errors caused by uncertainties in the wind forcing.

To specify the error model for transport estimates, we assume that transport uncertainties related to wind forcing σ_τ and diffusion σ_d are uncorrelated and provide two major contributions to the net transport error $\sigma_t = (\sigma_\tau^2 + \sigma_d^2)^{1/2}$. The values of σ_τ and σ_d were found as RMS deviations of the transport values from their means in the corresponding sensitivity experiments. The values of σ_t were computed for the transports of mass, heat, and salt across all the key sections in Ω. Their typical values range within 1-2 Sv, 0.1-0.2 PW, and 0.03-0.1 Tg s^{-1} (1Tg$\equiv 10^{12}$ g) for the mass, heat, and salt transports, respectively.

3. Circulation in Indonesian Seas

3.1. Consistency With Observations

Figure 5 shows the typical vertical distribution of the errors in potential temperature $\sigma'(\theta - \theta_c)$ and salinity $\sigma'(S - S_c)$ for a diagnostic pattern. Solid and short-dashed lines provide the RMS spatial variability for

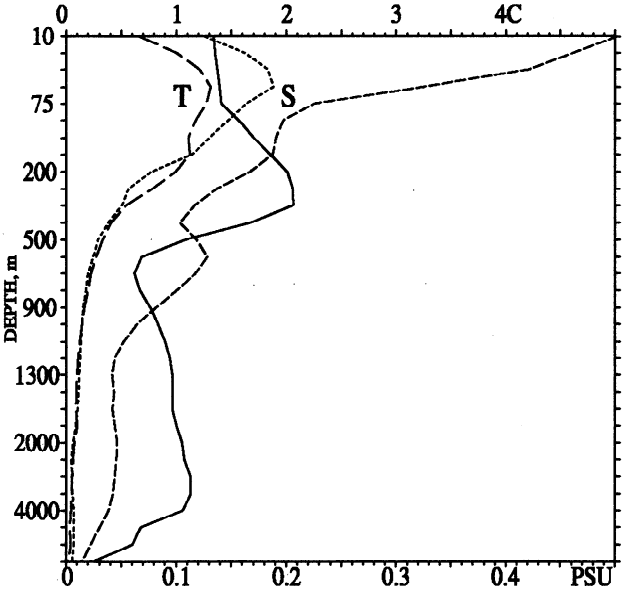

Figure 5. Vertical distributions of $\sigma(\theta_c)$, and $\sigma(S_c)$ for the *Levitus and Boyer* [1994] climatology (solid and short-dashed lines, respectively). The values of $\sigma(\theta - \theta_c)$ and $\sigma(S - S_c)$ for the diagnostic run with the RHR annual mean climatology (long-dashed and dotted lines, respectively).

Table 3. Total ITF Transports of Mass, Heat, and Salt Diagnosed With HR Climatology Using Different Diffusion Coefficients

K_m, 10^{-3}m^2 s^{-1}	$K_{\theta,S}$, 10^{-4}m^2 s^{-1}	D_m, 100 m^2 s^{-1}	$D_{\theta,S}$, 100 m^2 s^{-1}	Mass, Sv	Heat, PW	Salt, Tg s^{-1}
1	1	10	2	12.6	0.91	0.44
1	1	10	4	13.2	0.95	0.46
1	1	10	10	14.1	0.98	0.49
0.4	1	4	2	12.6	0.90	0.44
2	1	4	2	12.9	0.91	0.45
1	10	4	2	11.7	0.71	0.41
	mean$\pm\sigma_d$			12.8±0.7	0.89±0.09	0.45±0.03

Levitus climatology within the area in Plate 2. The largest deviations from the climatology are observed in the upper layer and do not exceed 1.3°C for potential temperature and 0.19 Psu for salinity. The mean relative error ϵ lies within the limits specified by the third error condition of section 2.3. We conclude that the diagnosed ocean state can be considered as consistent with climatological observations.

Another question is connected with the internal consistency of the diagnostic scheme. Using the technique described above, we implicitly assume that our "diagnostic operator," which projects climatologies onto the ocean state (result of the diagnosis), commutes with the time-averaging operator. If it were true, monthly and seasonal diagnoses, when averaged over the year, should give the result of the diagnosis for the annual mean climatology.

Table 4 displays mutual correspondence between the ITF transports computed via the adjustment of annual HR climatologies and the annually averaged transports produced by the four seasonal climatologies and 12 monthly climatologies. All three components of the net ITF transports demonstrate high consistency in the sense of the error bars outlined in section 2.3.

Total transport constituents computed for the 10 straits shown in Plate 2 also demonstrate high consistency within the framework of the above-mentioned error model. In the foregoing seasonal cycle analysis we shall describe only the diagnostic results corresponding to RHR climatology (line 2 in Table 2) because its values lie in-between the results obtained for other climatologies and therefore can be considered as the "most probable."

Table 4. Total ITF Transports of Mass, Heat, and Salt Obtained by the Annual Average of the Results Computed for Monthly and Seasonal RHR Climatologies

	Monthly	Seasonal	Annual
Mass, Sv	10.6±1.1	10.5±1.1	11.0±1.1
Heat, PW	0.74±0.10	0.73±0.10	0.79±0.10
Salt, Tg s^{-1}	0.37±0.04	0.37±0.04	0.39±0.04

3.2. Velocity Field and Transports

In order to monitor the ITF structure we selected 10 key sections in correspondence with the analysis by *Potemra et al.* [1997]. The "mean inflow" into the Indonesian seas is defined by the currents through the Karimata, Makassar, Molucca, Manipa, and Ceram Straits (Plate 2 and Table 1). The inflowing waters exit through the Lombok, Komodo, Lomblen, Ombai and Timor Straits. In contrast to configuration of the 0.4° POCM model analyzed by *Potemra et al.* [1997], we have closed the Torres and Sunda Straits, which have negligible cross-section areas according to ETOP05 data. Additionally, two relatively shallow straits (Komodo and Lomblen) were added because of the enhanced horizontal resolution.

Figure 6 displays seasonal variability of the mass transports through these two groups of straits. Although the values of total transport through the most of the inflow straits occasionally turn negative (northward), we shall follow this classification for convenience further below. Since the net magnitude of the total transport through the Komodo and Lomblen Straits never exceeded 2 Sv, we have added their values to the Ombai transport for brievity.

As can be seen from Figure 6, inflow transports are operating "in phase," having maxima in the second half of the year and minima in January–March. In winter and spring, transports through the three eastern straits are even negative, indicating the northward outflow into the Irian Java basin at the rate of 2–4 Sv. Transport through the westmost strait between Sumatra and Kalimantan is oppositely phased, having the maximum southward flow of 4.9±0.5 Sv in winter and being negligible (-0.2±0.6 Sv) in June–August.

Seasonal variability of the outflow has the analogous structure: four western straits operate approximately in phase with the maximum transports of 4–6 Sv in July–September and minima of 0–3 Sv in January–March. In contrast to the inflow, the "oppositely phased" is the eastmost passage between Timor and Australia. Its transport reaches a minimum of 1.6±0.6 Sv in September–October and has the maximal strength of 3.5±1.2 Sv in December–January (Figure 6b).

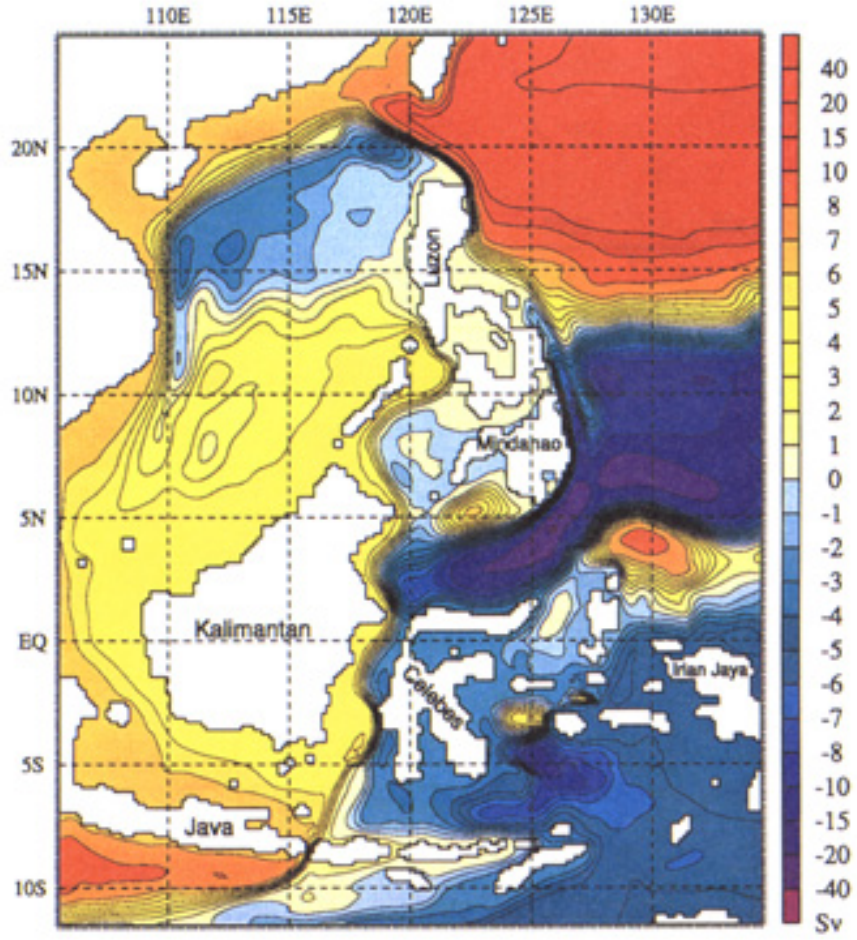

Plate 3. Annual mean stream function of total transport (sverdrups). Contours are labeled in sverdrups.

The net ITF transport is also shown in Figure 6b. Its annual average amounts to 11.0±1.2 Sv. Seasonal variability of the total ITF transport demonstrates a consistency with the one computed using *Godfrey*'s [1989] island rule.

Spatial distribution of the net flow within Ω is represented in Plates 3–4. These patterns were obtained via the ensemble average over the diagnoses of the six wind stress climatologies (Table 2). Despite the considerable eddy activity of the model most of the features present on these maps are persistent, and we consider them as confident for quantitative considerations.

The general circulation pattern shown in Plate 3 demonstrates the stream function of total transport obtained through diagnostic analyses of the annual mean climatologies. An interesting feature seen in Plate 3 is the importance of the flow between Luzon and Taiwan in the net ITF mass balance. The map demonstrates that more than half (6.2 Sv out of 11.5) of the ITF originates in that area. The Luzon inflow joins the cyclonic gyre in the South China Sea and bifurcates farther downstream at 10°N. The major part of the inflow (3.9±1.0 Sv) follows the route though the Mindoro Strait at 120°E, 13°N and then farther on until it joins a powerful stream (8 Sv), which can be viewed as an extension of the Mindanao current. Another bifurcation point is seen at the entrance to the Makassar Strait (1°N), where 7.2±1.1 Sv of the newly formed meridional jet continue farther south, while the remaining 4.7±1.5 Sv flow east along the northern coast of Celebes. Eventually, this current joins anticyclonic circulation within Halmahera Eddy and goes farther east into the equatorial Pacific. On the other hand, a flow of 2.0±0.8 Sv feeds ITF by the Pacific waters north of Irian Jaya. A considerable part (2.3±0.5 Sv) of the Luzon inflow follows all the way south through the shallow southern part of the South China Sea, enters the Java Sea, and finally, reaches the Lombok Strait. The total transport derived from the ensemble of annual climatologies amounts to 11.5±1.1 Sv.

The role of Luzon Strait in the net ITF mass balance has been noted in a number of modeling studies. *Metzger and Hurlburt* [1996] obtained the Luzon Strait transport varying from 4 to 12 Sv in the 1/2° Navy layered ocean model. They also diagnosed strong dependence of the transport on friction and geometry

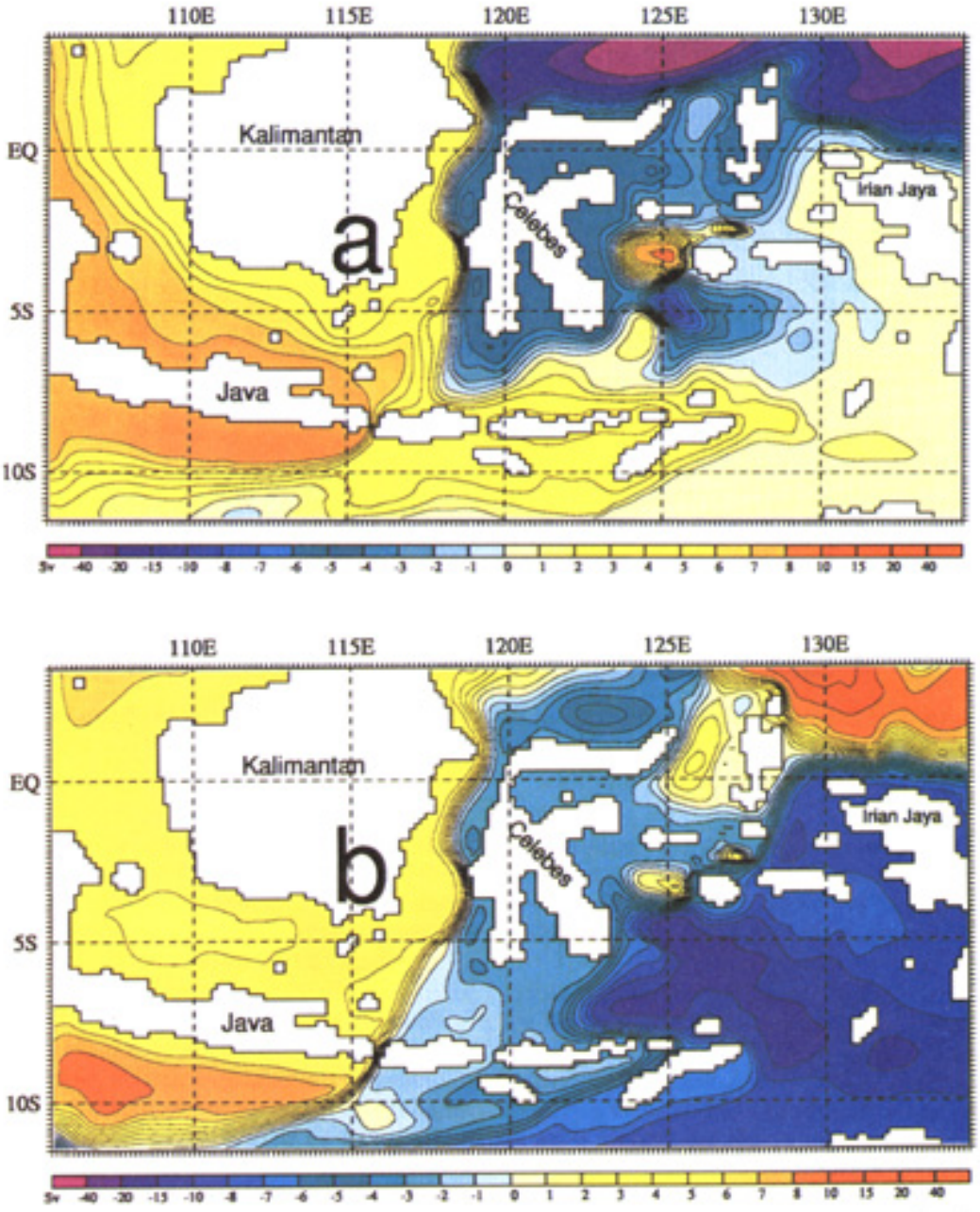

Plate 4. Climatological mean (a) winter and (b) summer distributions of the stream function in the Indonesian seas. Contours are labeled in sverdrups.

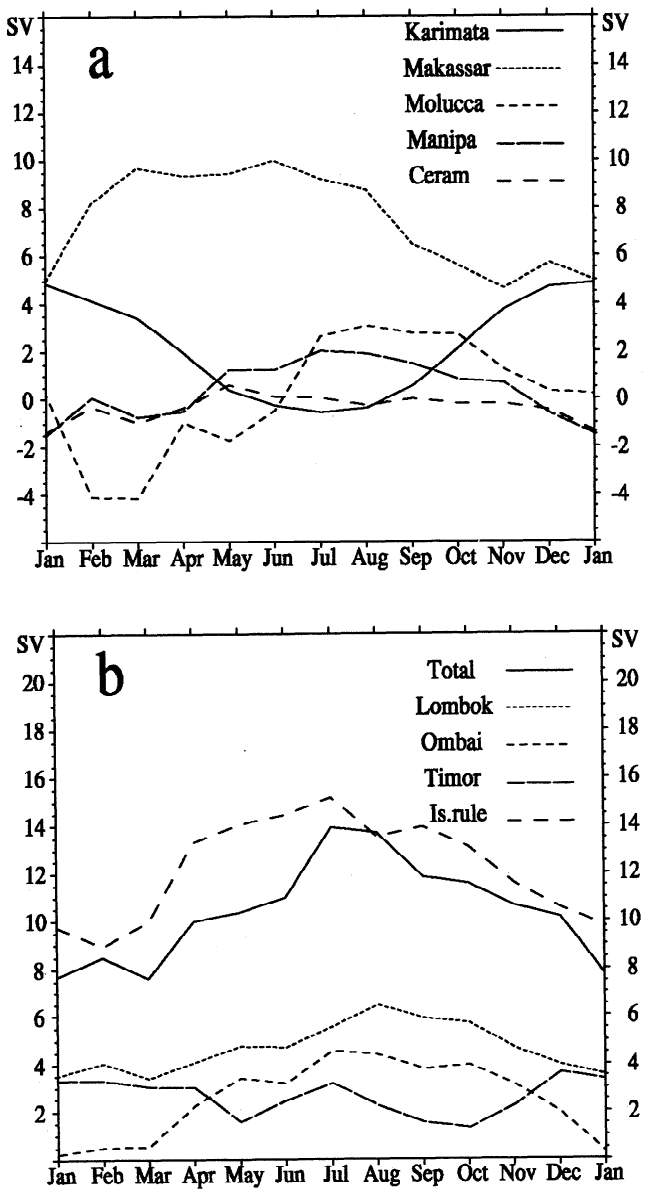

Figure 6. Seasonal evolution of the net mass transports through the (a) inflow and (b) outflow straits. The solid line in Figure 6b corresponds to the net ITF estimated by *Godfrey's* [1989] island rule for RHR winds.

of the Indonesian archipelago. *Wajsowicz* [1996] has shown that archipelago throughflow tends to follow the westmost pathway up to a certain friction-determined limit. In the absence of friction, *Wajsowicz* [1999] has obtained an inflated westward flow through the Luzon Strait and South China Sea. Some indications of the importance of the South China Sea route are also given by *Wyrtki* [1961] and *Miyama et al.*, [1995, 1996]. Since our result is stable with respect to viscosity and diffusivity variations, we attribute the higher contribution of the Luzon Strait to the finer resolution of the model grid, which now adequately resolves the Karimata and Mindoro passages. It is also interesting that in contrast to previous studies made with coarser resolution, the annual mean outflow through the Lesser Sunda Straits is more or less evenly distributed among the major passages (Plate 3).

Considering the seasonal cycle, we shall focus on the diagnosis of seasonal climatologies, having in mind that they do represent the major qualitative circulation features obtained by averaging the corresponding monthly patterns. Judging by the results presented in Figure 6, the key seasons are winter and summer. They have approximately opposite wind patterns (Figures 1a and 1b), which seem to define entirely the seasonal variability.

In winter, strong northwesterly winds enforce the flow from the South China Sea through the strait between Sumatra and Kalimantan. Total transport of that flow reaches 4.9±0.5 Sv in January (Figures 1a and 6a). At the same time, eastward winds in the Java Sea and north of Lesser Sunda Islands substantially reduce the southward transport from "inflowing" straits (Figure 6a) and create a high SSH anomaly in the Banda and northern Arafura Sea, which is clearly visible in TOPEX/Poseidon altimetry (Plate 5a). The winter transport pattern (Plate 4a) demonstrates that most of the Makassar inflow deviates eastward. The major part of that flow (4.5±1.5 Sv) recirculates around Celebes and through the Moluccas and eventually exits to the Pacific. This feature has been qualitatively obtained in the diagnostic study of *Miyama et al.* [1995].

In summer (Plate 4b) the winds are more favorable to force the flow through the Lesser Sunda Straits. On the other hand, they tend to block the inflow from the Karimata Strait and destroy the bifurcation point west of South Vietnam. During that season the excess waters from the Luzon Strait take the Mindoro Strait route, so that the transport through that passage increases from 1.9±1.5 Sv in winter to 4.7±0.6 Sv. The southward stream along 120°E amplifies up to 8.1±0.7 Sv and exits through the Lombok (6.4±0.4 Sv), Komodo (0.9±0.6 Sv), and Lomblen (2.0±0.4 Sv) Straits. Outflow passages east of Komodo are fed in summer by extremely warm waters from the Pacific warm pool north of Irian Jaya, with a net transport of 6.0±1.0 Sv. The Timor Passage outflow turns out to be 1.5 Sv smaller than in winter.

3.3. Heat and Salt Fluxes

The vivid difference between summer and winter circulation patterns results in a much higher seasonal signal of the heat transport. Figure 7 demonstrates variability of the mass and heat transports above and below 175 m. As can be seen, most of the variability is confined to the upper layer.

Following *Gordon and McClean* [1999], the heat transport has been computed relative to 2.8°C, which is the spatially averaged temperature of the return flow between Australia and Antarctica. The largest seasonal variability (0.8 PW in amplitude) occurs in the Molucca Strait, where the net heat transport reverses

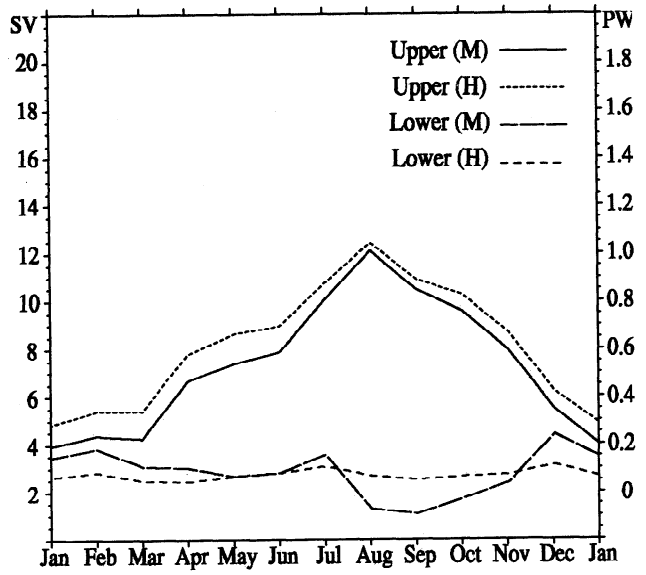

Figure 7. Seasonal evolution of the total ITF mass (M) and heat (H) transports. Upper transports were computed for the layer 0–175 m. The lower layer shows contribution to the transports from the layers below 175 m.

in sign twice a year, corresponding to switches between the summer and winter regimes (Figure 8). The annual mean net transport averages 0.83±0.10 PW, with an amplitude of seasonal variations of 0.4 PW.

Salt transports are quite similar to the curves of the net mass transports because of much lower relative variations in salinity. The annual mean salt flux into the Indian Ocean is diagnosed as 0.40± 0.04 Tg s^{-1}, with seasonal variation of 0.1 Tg s^{-1}.

4. Correlation With TOPEX/Poseidon Altimetry

Robust diagnostics of the net ITF property transports with remote sensing data and long-term in situ observations is an interesting subject that has been addressed in recently by *Potemra et al.* [1997] and *Murtugudde et al.* [1998]. The idea of correlation between ITF transport anomalies and SSH dates back to the work of *Wyrtki* [1961], who supposed that the net transport is proportional to the large scale pressure difference between the Pacific and Indian Ocean basins. Using a low-order autoregressive analysis, *Potemra et al.* [1997] obtained an index, quantifying the POCM ITF transport via a linear combination of SSH measurements at the coasts of Philippines, Australia, Java, and New Guinea. The correlation was found to be ~0.78. *Murtugudde et al.* [1998] established a correlation of 0.75 between the Java–New Guinea TOPEX/Poseidon (T/P) SSH difference and ITF in their 1/3° model.

That a significant portion of the transport between Luzon and Taiwan contributes to the net ITF was shown in section 3.2. Besides, T/P SSH anomalies demonstrate a clear dipole structure with "charges" located near Luzon and in the eastern Banda Sea (Plate 5). Good correspondence of the ITF transport variability to the transport variability diagnosed only by winds (Figure 6b) indicates that the heuristic approach should also account for wind stress variability, which may be responsible for creating the above-mentioned SSH anomaly structure.

Figure 9 shows the temporal evolution of SSH anomaly difference between the Luzon and eastern Banda Sea regions taken from T/P altimetry $\delta\zeta_{T/P}$ and from the diagnostic runs with monthly RHR climatologies $\delta\zeta_m$. Here $\delta\zeta_{T/P}$ was obtained by taking the mean differences of T/P anomalies over 5 years of observation (1993–1997). The region boundaries corresponding to the Luzon and Banda Sea maxima were selected as 117°–120°E, 18°–21°N, and 130°–133°E, 5°–8°S. As

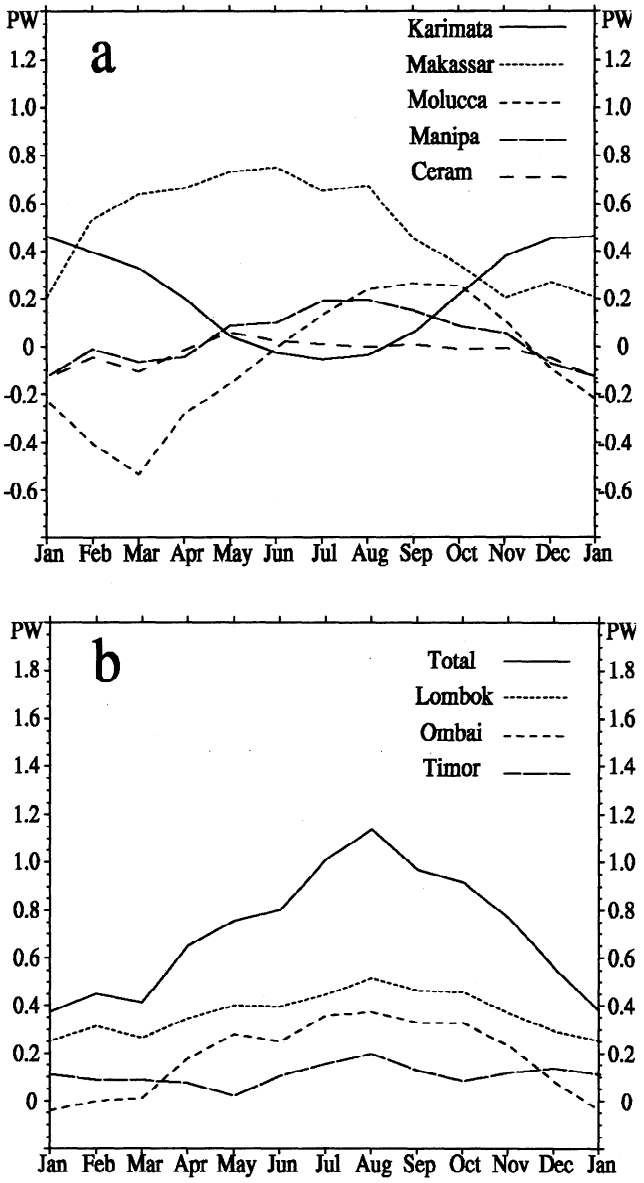

Figure 8. Seasonal evolution of the heat transports through the (a) inflow and (b) outflow straits.

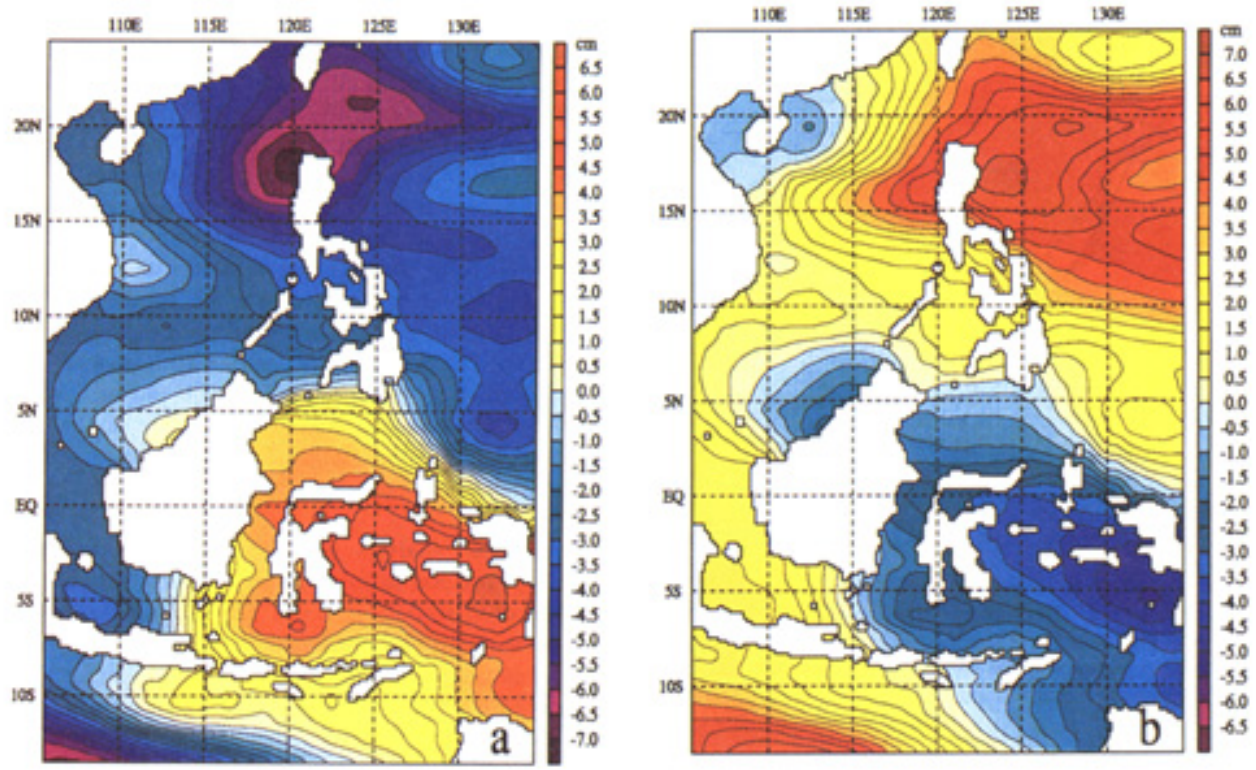

Plate 5. TOPEX/Poseidon SSH anomalies computed as average deviations from the 5 year (1993–1997) mean in (a) winter (January–March) and (b) summer (July–Sepember). Contours are labeled in centimeters.

can be seen from Figure 9, the diagnostic values of the ITF transport are very close to the SSH difference curve taken from the model (correlation 0.94). Further improvement of the correlation coefficient can be done by introducing an additional degree of freedom into the linear operator, projecting $\delta\zeta_{T/P}$ onto the ITF transport (the technique used by *Potemra et al.* [1997]). Experiments of this type have shown that correlation between ITF transport and "indexed" T/P altimetry can reach 0.95 if T/P anomaly values in the regions west of Mindanao and south of western Java are taken into account.

Even higher correlation is observed with the heat transport, whose maximum is lagging behind the ITF mass transport by 1 month. The curves shown in Figure 9 correlate at the level of 0.96, while the above mentioned T/P altimetry index was found to correlate with the heat transport at the 0.97 level.

This strong correlation can partly be explained by the larger contribution to ITF of the Luzon Strait transport and by the fact that seasonal ITF variability is confined to the upper layer (Figure 7) and therefore primarily caused by SSH variations. Our computations may be viewed as a support of the results of *Metzger and Hurlburt* [1996], who suggested that seasonal variability of the Luzon Strait transport is controlled by the pressure head created by the pileup of water from the monsoonal winds. In the eastern Banda Sea this "pileup mechanism" should have the opposite phase (see Figures 1a and 1b), and it does have, as is demonstrated by T/P observations in Plates 5a and 5b. In reality, seasonal variability of the ITF transport depends on a large number of factors, such as friction in the numerous straits, Kelvin wave statistics within the archipelago, tidal effects, and so on. Our diagnostic computations suggest that the primary driving mechanism is the monsoonal wind variability, which causes the associated changes in SSH. Taking into account strong correlation of the model SSH with T/P altimetry, we can also state that the Luzon Strait "northern route" may provide a considerable contribution to the total ITF transport.

5. Discussion and Conclusions

The mean seasonal variability of the Indonesian Throughflow has been studied on a 1/6° grid by a diagnostic method using the wind stress and hydrographic climatologies. Compared to previous diagnostic and modeling studies of the throughflow, we have made an attempt to put more emphasis on data, avoiding the long-term integrations of model equations forced by relatively uncertain winds and thermohaline fluxes at the sea surface and/or artificial 3-D sources of heat and salt. The diagnosed monthly mean states of the Indonesian Throughflow lie within the error bars of the

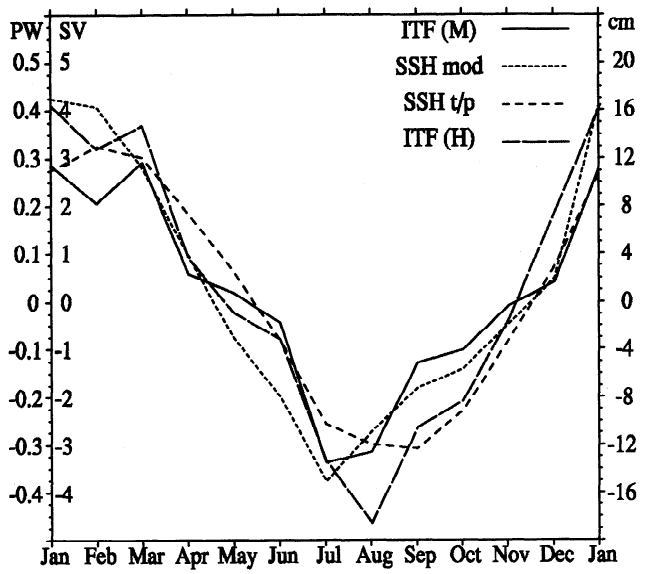

Figure 9. Mean seasonal evolution of the SSH difference between the regions near Luzon and western Banda Sea as seen by TOPEX/Poseidon (SSH t/p) and by model diagnosis (SSH mod) and the evolution of the diagnosed ITF mass (M) and heat (H) transports.

Levitus and Boyer [1994] climatology and are dynamically consistent. Additionally, a large set of sensitivity experiments has been conducted. Six different wind climatologies were used to test ITF sensitivity to the errors in wind stress. It was found that the annual mean ITF transport varies by 0.8 Sv (7% of its magnitude), while the RMS deviation of the wind climatologies from their mean reaches 10–15% of their typical magnitudes in the ITF region.

Special emphasis has been made to accurately define of the model topography, which is more realistic than that in the latest studies known in literature. For instance, the 0.4° configuration of the global GCM by *Semtner and Chervin* [1992], whose output was studied by *Potemra et al.* [1997], suffers from a poorly resolved Lombok Strait and an unrealistically deep Torres Strait. Alternatively, in a 1/2° diagnostic study of *Miyama et al.* [1995], the Lombok Strait cross-section area was strongly overestimated. *Gordon and McClean* [1999] in their recent analysis of the 1/4° configuration of the Los Alamos National Laboratory GCM also mention crucial topographic deficiencies, such as a too wide Torres Strait [*Gordon and McClean*, 1999, p. 215], "through which the model permits an unrealistically large exchange between the Coral Sea and Indonesian seas." In our model configuration all these deficiencies have been removed on the basis of ETOP05 topography.

The refined horizontal and vertical resolution enabled us to obtain more accurate tracking of the throughflow transport. In particular, more distinct quantification of the ITF component through the South China Sea route has been obtained. The importance of that flow in the total ITF mass budget was first noticed by *Masumoto and Yamagata* [1993] and further quantified in the diagnostic study of *Miyama et al.* [1995], who estimated the relative contribution of the Karimata Strait transport as 12%, with the rest being supplied by the Mindanao current on the annual average. Our computations indicate that South China Sea waters contribute 85% to the total throughflow in winter and ~50% on the annual average. We attribute this result to better resolution of the Mindoro and Karimata passages, connecting the South China Sea with the Java and Sulu Seas. Another novel feature of the ITF patterns is the somewhat more homogeneous distribution of the outflow among the Lesser Sunda Straits. We assume that this finding is entirely due to the better resolution of topography.

Correlation analysis of the ITF transports and TOPEX/Poseidon altimetry has revealed a high correlation of 0.91–0.95 between the difference of SSH anomalies north of Luzon and anomalies in the eastern Banda Sea. These values are somewhat larger than those obtained by previous researchers who prescribed the "Indian basin SSH anomalies" to the regions south of Java [*Murtugudde et al.*, 1998] and east of Timor [*Potemra et al.* 1997]. The major reason for larger correlations is due to the fact that we were aimed at finding the largest possible correlation between the model "Indo-Pacific SSH difference" and ITF anomalies. The regions providing this largest correlation are found to coincide with the regional maxima of the mean seasonal SSH anomalies as seen by T/P satellite in the period between 1993 and 1998. One of that regions seems to be responsible for the seasonal cycle of the Luzon Strait transport, indicating its possible importance in the total ITF mass balance.

Many features of the ITF seasonal variability obtained in the present paper have been documented recently by others [e.g., *Metzger and Hurlburt*, 1996, *Miyama et al.*, 1995] who utilized coarser-resolution models. Our findings can be viewed as further quantification of the ITF structure obtained by an alternative diagnostic approach. The major results are as follows.

1. The Luzon Strait inflow is shown to give a considerable contribution to ITF. In winter the inflow of 6.3±1.5 is distributed between the two outflows from the South China Sea that follow the pathways through Karimata (4.4±0.5) and Mindoro (1.9±1.5 Sv) Straits to Lesser Sunda passages at 8.5°S. In summer the Karimata pathway is blocked (-0.2±0.6 Sv), and the net inflow of 4.7±0.6 Sv exits through the Mindoro Strait west of southern Luzon.

2. In contrast to previous studies, which used coarser topographies, the ITF outflow is shown to be more evenly distributed among the passages through Lesser Sunda Islands. On the annual mean, 5.4±0.3, 3.5±0.3, and 2.6±0.8 Sv exit through the Lombok,

Komodo-Ombai, and Timor Straits, respectively. The largest seasonal variability (0–4.5 Sv) is observed in the Komodo–Ombai passages.

3. In winter the total transport pattern is characterized by the strong deflection of the Makassar Strait outflow of 7.6±1.7 Sv to the east, where 4.5±1.5 Sv of that outflow recirculates around Celebes through the Moluccas and enters the Pacific warm pool north of Irian Jaya.

4. The model SSH difference between the eastern Banda Sea and northwest of Luzon strongly correlates with TOPEX/Poseidon SSH monthly anomalies averaged over 5 years, 1993–1997. The correlation coefficients between the net ITF transports of mass, heat, and salt and T/P SSH anomalies are 0.91, 0.96, and 0.90, respectively.

5. The total annual mean ITF transports of mass, heat, and salt are diagnosed as 11.5±1.1 Sv, 0.83±0.10 PW, and 0.40±0.04 Tg s^{-1}. Their seasonal variability is characterized by minima in boreal winter and maxima in boreal summer. Amplitudes of these oscillations are 3.2 Sv, 0.4 PW, and 0.1 Tg s^{-1}, respectively.

Acknowledgments. This study was supported by the Frontier Research System for Global Change through its sponsorship of the International Pacific Research Center (IPRC), NASA grant NAG5-7485, and Russian Foundation for Basic Research grant 99-05-65484. The Center for Space Research of the University of Texas at Austin is acknowledged for providing the preprocessed TOPEX/Poseidon data. Helpful discussions with H. Mitsudera, T. Miyama and J. Potemra are acknowledged. This manuscript is SOEST contribution 4967 and IPRC contribution IPRC-37.

References

Da Silva, A., C. C. Young, and S. Levitus, Atlas of surface marine data, in *NOAA Atlas NESDIS 6*, Natl. Oceanogr. Data Cent., Silver Spring, Md., 1995.

Demin, Y. L., and R. A. Ibraev, A numerical method for calculation of currents and sea surface topography in multiply connected domains, *Sov. J. Num. Analy. Math. Model.*, *4*, 179–252, 1989.

Dukowicz, J. K. and R. D. Smith, Implicit free-surface method for the Bryan-Cox-Semtner ocean model, *J. Geophys. Res.*, *99*, 7991-8014, 1994.

Dukowicz, J. K., R. D. Smith, and R. C. Malone, A reformulation and implementation of the Bryan-Cox-Semtner ocean model on the connection machine, *J. Atmos. Oceanic Technol.*, *10*, 195-208, 1993.

Godfrey, J. S., A Sverdrup model of the depth-integrated flow for the world ocean allowing for island circulations, *Geophys. Astrophys. Fluid Dyn.*, *45*, 89-112, 1989.

Goerss, J. S., and P. A. Phoebus, The navy's operational atmospheric analysis, *Weather Forecasting*, *7*, 232-249, 1992.

Gordon, A. L., and J. L. McClean, Thermohaline stratification of the Indonesian seas: Model and observations, *J. Phys. Oceanogr.*, *29*, 198–216, 1999.

Hellerman, S., and M. Rosenstein, Normal monthly wind stress over the world ocean with error estimates, *J. Phys. Oceanogr.*, *13*, 1093–1104, 1983.

Inoue, M., and S. E. Welsh, Modeling seasonal variability in the wind-driven upper-layer circulation in the Indo-Pacific region, *J. Phys. Oceanogr.*, *23*, 1411–1436, 1993.

Ivanov, Y. A., K. V. Lebedev, and A. S. Sarkisyan, Generalized hydrodynamic adjustment method, *Izv. Russ. Acad. Sci. Atmos. Oceanic Phys.*, *33*, 752–757, 1997.

Ishizaki, H. , A simulation of the abyssal circulation in the North Pacific Ocean, *J. Phys. Oceanogr.*, *24*, 1941-1954, 1994.

Levitus, S., and T. P. Boyer, World ocean atlas 1994, vol.3-4, in *NOAA Atlas NESDIS 3-4*, U.S. Dept. of Comm., Washington, D.C., 1994.

Masumoto, Y., and T. Yamagata, Simulated seasonal circulation in the Indonesian seas, *J. Geophys. Res.*, *98*, 12,501-12,509, 1993.

Masumoto, Y., and T. Yamagata, Seasonal variations of the Indonesian Throughflow in a general ocean circulation model, *J. Geophys. Res.*, *101*, 12,287-12,294, 1996.

Metzger, E. J., and H. E. Hurlburt, Coupled dynamics of the South China Sea, the Sulu Sea, and the Pacific Ocean, *J. Geophys. Res.*, *101*, 12,331-12,352, 1996.

Miyama, T., T. Awaji, K. Akimoto, and N. Imasato, Study of seasonal transport variations in Indonesian seas, *J. Geophys. Res.*, *100*, 20,517-20,541, 1995.

Miyama, T., T. Awaji, K. Akimoto, and N. Imasato, A Lagrangian approach to the seasonal variability of salinity in the mixed layer of the Indonesian seas, *J. Geophys. Res.*, *101*, 12,265-12,285, 1996.

Murtugudde, R., A. G. Busalacchi, and J. Beauchamp, Seasonal-to-interannual effects of the Indonesian throughflow on the tropical Indo-Pacific basin, *J. Geophys. Res.*, *103*, 21,425–21,441, 1998.

National Oceanic and Atmospheric Administration (NOAA), ETOP05 digital relief of the surface of the Earth data announcement, *NOAA Tech. Rep.* 86-MGG-07, Nat. Geophys. Data Cent., Washington, D.C., 1986.

Pitcher, E. J., R. C. Malone, V. Ramanathan, M. L. Blackmon, K. Puri, and W. Burke, January and July simulations with a spectral general circulation model, *J. Atmos. Sci.*, *40*, 580–604, 1983.

Potemra, J. T., Seasonal variations of the upper ocean transport from the Pacific to the Indian Ocean via Indonesian Straits, *J. Phys. Oceanogr.*, in press, 2000.

Potemra, J. T., R. Lukas, and G. T. Mitchum, Large-scale estimation of transport from the Pacific to Indian Ocean, *J. Geophys. Res.*, *102*, 27,795–27,812, 1997.

Sarmiento, J. L., and K. Bryan, An ocean transport model for the North Atlantic, *J. Geophys. Res.*, *87*, 394-408, 1982.

Schiller, A., J. S. Godfrey, P. C. McIntosh, G. Meyers, and S.E. Wiffles, Seasonal near-surface dynamics and thermodynamics of the Indian Ocean and Indonesian Throughflow in a global ocean circulation model, *J. Phys. Oceanogr.*, *28*, 2288–2312, 1998.

Schneider, N., and T. P. Barnett, Indonesian Throughflow in a coupled general circulation model, *J. Geophys. Res.*, *102*, 12,371–12,358, 1997.

Semtner, A. J., and R. M. Chervin, Ocean general circulation from a global eddy-resolving model, *J. Geophys. Res.*, *97*, 5493-5550, 1992.

Smith, R. D., J. K. Dukowicz, and R. C. Malone, Parallel ocean general circulation modeling, *Physica D*, *60*, 38-61, 1992.

Stockdale, T., D. Anderson, M. Davey, P. Delecluse, A. Kattenberg, Y. Kitamura, M. Latif, and T. Yamagata, Intercomparison of tropical ocean GCMs, *Publ. WCRP-79 WMO/TD 545*, 90 pp., World Clim. Res. Program, World Meteorol. Org., Geneva, 1993.

Trenberth, K. E., J. G. Olson, and W. G. Large, A global

ocean wind stress climatology based on ECMWF analyses, *NCAR Tech. Note NCAR/TN-338+ STR*, 93 pp., Natl. Cent. for Atmos. Res., Boulder, Colo., 1989.

Trenberth, K. E., W. G. Large, and J. G. Olson, The mean annual cycle in global ocean wind stress, *J. Phys. Oceanogr., 20*, 1742-1760, 1990.

United Nations Educational Scientific, and Cultoral Organization (UNESCO), Tenth report of the joint panel on oceanographic tables and standards, *UNESCO Tech. Pap. Mar. Sci., 36*, 25 pp., 1981.

Wajsowicz, R. C., Flow of a western boundary current through the multiple straits: An electrical circuit analogy for the Indonesian Throughflow and archipelago, *J. Geophys. Res., 101*, 12,295-12,300, 1996.

Wajsowicz, R. C., Models of the south Asian seas, *J. Phys. Oceanogr., 29*, 986-1018, 1999.

Washington, W. W., and C. L. Parkinson, *An Introduction to Three-Dimensional Climate Modeling.*, Oxford Univ. Press, New York, 1986.

Wyrtki, K., Physical oceanography of the southeast asian waters, *NAGA Rep. 2*, Scripps Inst. of Oceanogr., La Jolla, Calif., 1961.

K. V. Lebedev and M. I. Yaremchuk, International Pacific Research Center, University of Hawaii, Honolulu, HI 96822. (klebedev@soest.hawaii.edu)

(Received May 21, 1999; revised January 20, 2000; accepted January 20, 2000.)